ROS2-Based End-to-End BCI Robot Control with Generative EEG Channel Restoration and Intent Classification

Youngwoong Youn

yuhyun9828@gmail.com

Key Words: Brain–Computer Interface (BCI), Electroencephalography (EEG), Channel Reconstruction, Conditional Diffusion Model, Motor Imagery Classification, ROS2, Mobile Robot / Wheelchair Robot, LiDAR-Based Obstacle Avoidance

Abstract: This study proposes a BCI robot control system that mitigates information loss in low-channel EEG-based BCI environments while reducing user burden by minimizing the number of electrodes, thereby enabling stable robot control. The proposed system takes MI-9 low-channel EEG signals from the BCI Competition IV Dataset 2a as input and restores full 22-channel EEG signals using a conditional diffusion-based generative model, compensating for the spatial neural information required for classification under constrained measurement conditions. Based on the restored EEG signals, motor imagery classification is performed, and the classification results are interpreted as user intent within a ROS2 environment and translated into robot control commands, establishing a continuous end-to-end connection between BCI and robotic control. In addition, a LiDAR-based safety filter is applied to decelerate or stop the robot in hazardous forward situations, ensuring environmental safety while preserving user intent. Simulation experiments validate the reproducibility of the proposed system and its collision avoidance performance.

1. Introduction

Brain–computer interfaces (BCIs) provide an alternative pathway for individuals with severe motor impairments to control robotic arms, assistive devices, and mobile robots.(1) In particular, non-invasive EEG-based BCIs are attractive due to their clinical feasibility and accessibility; however, they inherently suffer from limitations in stable intent inference and long-term operation caused by low signal-to-noise ratio (SNR), inter-subject variability, and inter-session non-stationarity.(2) Nevertheless, recent studies have demonstr -ated that continuous-level robot control is achievable using non-invasive signals alone, thereby accelerating the transition of BCI technologies toward real-world usage scenarios.(3)

One of the most critical practical bottlenecks hindering the deployment of BCIs is the user burden associated with an increasing number of electrodes or channels. While high-density EEG provides richer spatial resolution, it significantly degrades usability in daily environments due to prolonged setup time, increased difficulty in electrode placement and alignment, contact impedance manageme -nt, and reduced mobility.(4) Consequently, approaches that can secure the information required for classification and control "with fewer electrodes" are essential. This challenge extends beyond signal processing optimization and directly translates into a system-level design problem aimed at improving user comfort and wearability. (5)

Reducing the number of EEG channels enhances wearability but inevitably leads to the loss of spatial patterns—particularly inter-channel relationships—that are critical for motor imagery (MI) classification, resulting in degraded classification performance and control stability.(6) This issue is not merely a matter of model accuracy; when propagated to robotic control, accumulated errors may escalate into safety risks. Furthermore, while BCI-based robot control must primarily reflect user intent, real-world environments require concurrent sensor-based hazard assessment. This necessitates an explicit definition of the boundary between "preserving user intent" and "safety intervention."

The objective of this study is to ensure stability and reproducibility at the system level, including robotic control, under the premise of electrode minimization through low-channel EEG observation. To this end, we propose a framework that: (1) restores multi-channel EEG representations from low-channel observations using a generative model to compensate for missing spatial information; (2) estimates user intent through motor imagery classification based on the restored EEG signals; (3) converts the inferred intent into robot control commands within a ROS2-based modular architecture; and (4) applies a LiDAR-based safety filter that intervenes

only by decelerating or stopping the robot in hazardous situations. Importantly, the safety filter is not designed to replace autonomous navigation but rather to preserve user intent by default while performing limited intervention exclusively in risk scenarios, thereby ensuring interpretabi -lity and experimental controllability.

The main contributions of this work are summarized as follows:

1. Channel restoration–based BCI pipeline for electrode minimization: Low-channel EEG signals (e.g., MI-9) are used as observations, while multi-channel representations (e.g., 22 channels) are restored via a conditional generative model to enrich the input information for the classification stage.

2. End-to-end integration of restoration, classification, and control: The entire processing chain—from EEG restoration and classification to ROS2-based control topics—is constructed in a modular manner to enhance reproducibility and extensibility.

3. Intent-preserving safety intervention architecture: Final robot velocity commands prioritize user intent, while a LiDAR-based safety filter enforces deceleration or stopping only when environmental hazards are detected, achieving a balance between intent preservation and environmental safety.

4. Simulation-based reproducibility validation framework: A reproducible experimental protocol is provided using Gazebo simulation and ROS2 logging, ensuring identical robot behavior under identical inputs and parameters.

By placing wearability constraints—specifically electrode count at the center of system design, this approach aligns with the broader trajectory of extending non-invasive BCIs toward robotic control while targeting practical usability improvements. Considering the widely recognized challenges of long-term stability and variability in BCI systems, the modular separation of restoration, classification, and safety control offers a favorable foundation for future extension to real-world, online EEG data.

2. Diffusion Model–Based EEG Channel Restoration

Diffusion-based generative models are formulated as probabilistic frameworks that generate samples through a forward diffusion process, in which the data distribution is gradually corrupted into Gaussian noise, and a reverse denoising process, in which the original data are reconstructed using a learned model.(7) Early diffusion probabilistic models were first systematically introduced from a nonequilibrium thermodynamics perspective, proposing the principle of "progressive noise injection and reverse-process learning," and were later refined through neural network–based parameterization and simplification of training objectives.(8)

In particular, denoising diffusion probabilistic models (DDPMs) implement the reverse diffusion process as iterative denoising steps and demonstrate high-quality generative performance through their connection to score matching, thereby accelerating the practical adoption of diffusion models. Subsequent advancements—including accelerated sampling techniques such as DDIM to reduce computational cost, model variants that improve generation quality, likelihood estimation, and sample efficiency, as well as guidance-based methods that control the quality–diversity trade-off in conditional generation—have extended diffusion models beyond image synthesis to a wide range of conditional generation and restoration tasks.(9)

More recently, the structural paradigm of "progressive restoration from noise" has been applied to time-series and biosignals. In this context, several studies have emerged that reformulate conditional restoration problems—such as channel interpolation and spatial super-resolution—in low signal-to-noise ratio and highly variable signals like EEG from a generative modeling perspective.(10)

2.1. Preprocessing and Input Construction

In this study, a consistent preprocessing pipeline was applied to the BCI Competition IV Dataset 2a (BCICIV_2a) to ensure stable training and reproducibility of the EEG channel restoration and motor imagery classification models. The objectives of preprocessing are threefold: (i) to improve the signal-to-noise ratio by removing noise and non-physiological artifacts, (ii) to construct a uniform input representation across all subjects and sessions, and (iii) to generate fixed-dimensional input tensors required by the generative and classification models. The entire preprocessing procedure was implemented using MNE-Python, a standard library for neurophysiological signal analysis, thereby ensuring

consistency and reproducibility across all signal processing stages.

The raw EEG data consist of 22 EEG channels and 3 EOG channels. To maintain spatial consistency in the model input, the EEG channel names and ordering were standardized to a canonical 22-channel configuration **(Figure 1)**. The EOG channels were explicitly designated with the eog channel type to facilitate the detection of ocular artifacts. Common average reference (CAR) was applied to all EEG signals, and a standard 10–20 system montage was used to align electrode locations. These referencing and montage settings provide a fundamental basis for stable comparison of relative potential distributions across channels **(Figure 2)**.

For frequency-domain preprocessing, notch filters at 50 Hz and 100 Hz were applied to suppress power-line noise, along with an 8–30 Hz band-pass filter targeting frequency bands predominantly associated with motor imagery–related rhythms. This filtering strategy attenuates low-frequency drift and high-frequency noise while emphasizing neural activity in the μ and β bands. Identical filtering was applied to both EEG and EOG channels, facilitating subsequent artifact separation during later processing stages.

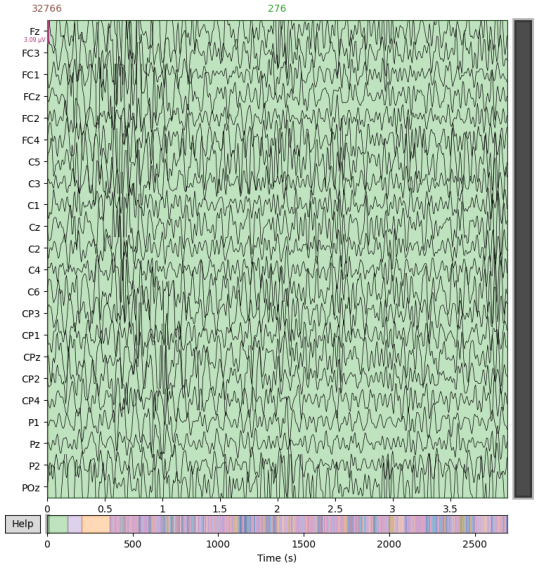

Fig. 1 Epoch definition and tensor representation used as model input. Each trial is segmented into a 4-second window and represented as a fixed-size tensor.

To reduce contamination caused by eye movements and eye blinks, the preprocessing pipeline includes an independent component analysis (ICA)–based artifact removal procedure. ICA was trained on the EEG channels, and ocular-related components were identified based on their correlation with the EOG channels. These components were subsequently removed to reconstruct artifact-reduced EEG signals. The application of ICA was controlled using a fixed random seed, ensuring that preprocessing results were reproducible under identical conditions.

To construct fixed-length, trial-wise input signals for model training, event-based epoching was performed. Each trial was defined to include a 0–4 s interval following stimulus onset, and no baseline correction was applied. The resulting epochs were labeled according to their corresponding motor imagery classes, and epochs generated from different sessions were merged into a single data array using a consistent format. Both subject-wise preprocessing outputs and the combined dataset were stored, enabling flexible reuse under different experimental configurations.

To ensure stable neural network training, z-score normalization was applied to all epoch signals. The normalized data were then reshaped into tensors of size $\boldsymbol{R^{N\times 1\times 22\times T}}$, where $\boldsymbol{N}$ denotes the total number of trials, 22 represents the number of EEG channels, and $\boldsymbol{T}$ is the number of temporal samples per epoch. The leading singleton channel dimension was included to match the input specifications of the subsequent PyTorch-based generative and classification models. Class labels were reindexed as integer values and normalized to the range [0,3].

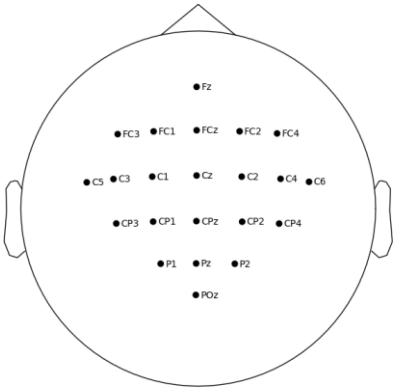

Fig. 2 EEG electrode mapping and spatial configuration.

Finally, the entire dataset was divided into training and evaluation sets using a stratified split to preserve class distribution. The split ratio and random seed were fixed to ensure that identical training and evaluation datasets could

be reproduced under the same preprocessing code and configuration. This preprocessing and input construction pipeline provides a consistent foundation for the comparative analysis of the conditional diffusion–based EEG channel restoration model and the motor imagery classification model presented in the subsequent sections, ensuring that both models operate under identical input assumptions.

2.2. Conditional Diffusion–Based EEG Channel Restoration Model

In this study, a conditional diffusion-based generative model is applied to the EEG channel restoration problem in order to reconstruct multi-channel EEG signals from low-channel observations. This task can be formulated as a conditional inverse problem, where only a subset of channels (MI-9) is observed, and the full 22-channel EEG time series must be estimated. Under such conditions, a probabilistic generative modeling approach is well suited to progressively recover the missing spatial information.

Diffusion models construct a latent distribution by gradually injecting Gaussian noise into the real data $\boldsymbol{x_0}$ through a forward diffusion process until reaching $\boldsymbol{x_T}$, and subsequently recover the original distribution by iteratively removing noise using a learned neural network in the reverse process. In this work, the full 22-channel EEG time series is defined as $\boldsymbol{x_0} \in \mathbb{R}^{\boldsymbol{22\times T}}$, and channel restoration is performed as a reverse diffusion process conditioned on the observed subset of channels.

To this end, we define an observed channel set $\boldsymbol{C_{obs}}$ and a missing channel set $\boldsymbol{C_{miss}}$. Following common practice in MI-based BCI settings, nine central channels (MI-9) are selected as $\boldsymbol{C_{obs}}$, while the remaining 13 channels are designated as the restoration target $\boldsymbol{C_{miss}}$. The observed signals are embedded into the full channel space to form a conditional input $\boldsymbol{x_{cond}}$, where the true EEG values are retained at the observed channel locations and zeros are filled elsewhere. In addition, a binary mask $\boldsymbol{m} \in \{\mathbf{0},\mathbf{1}\}^{\boldsymbol{22\times T}}$ is defined to explicitly indicate channel observability, taking a value of 1 at observed channel locations and 0 otherwise.

The forward diffusion process is defined as

$$\boldsymbol{q(x_t \mid x_0) = \mathcal{N}(x_t; \sqrt{\bar{\alpha}_t}x_0,\ (1-\bar{\alpha}_t)\mathbf{I})},$$

Where, $\{\boldsymbol{\beta_t}\}_{\boldsymbol{t=1}}^{\boldsymbol{T}}$ denotes a linearly scheduled noise variance, $\boldsymbol{\alpha_t = 1-\beta_t}$, and $\boldsymbol{\bar{\alpha}_t = \prod_{s=1}^{t}\alpha_s}$. During training, a noise sample $\boldsymbol{\epsilon \sim \mathcal{N}(0,\mathbf{I})}$ is drawn at a randomly selected time step $\boldsymbol{x_t}$.

The reverse process is implemented via a noise prediction network $\boldsymbol{\epsilon_\theta(\cdot)}$, which explicitly incorporates both the conditional input and the mask. Specifically, the model input is constructed as

$$\boldsymbol{input = [x_t,\ x_{cond},\ m] \in R^{66\times T}}$$

corresponding to (i) the current noisy full-channel EEG signal, (ii) the conditional signal containing only observed channels, and (iii) the channel-wise observation mask concatenated along the channel dimension. This formulation enables the model to explicitly recognize which channels are observed and which must be restored during the denoising process.

The noise prediction network is designed as a one-dimensional convolutional architecture that preserves temporal resolution. To maintain temporal continuity of the EEG time series, no downsampling or upsampling operations are employed. Instead, expressive capacity is achieved through multi-stage convolutional blocks with residual connections. The diffusion time step $\boldsymbol{t}$ is embedded using sinusoidal time embeddings and injected into each residual block, allowing the model to learn noise-level–dependent conditional denoising. The final output is a noise estimate $\boldsymbol{\hat{\epsilon}_\theta \in R^{22\times T}}$ for all EEG channels.

Training follows the standard DDPM objective, minimizing the mean squared error (MSE) between the true noise $\boldsymbol{\varepsilon}$ and the predicted noise $\boldsymbol{\hat{\epsilon}_\theta}$:

$$\boldsymbol{L_{DDPM} = E_{x_0,\epsilon,t}[\| \epsilon - \hat{\epsilon}_\theta(x_t, x_{cond}, m, t) \|_2^2]}.$$

This loss is computed over all channels without explicitly distinguishing observed and missing channels, while the observed-channel information is implicitly enforced through the conditional input and mask.

During inference, reverse diffusion is performed using only the observed MI-9 channels to reconstruct the full 22-channel EEG. The initial state $\boldsymbol{x_T}$ is sampled from Gaussian noise, and $\boldsymbol{x_{t-1}}$ is computed at each reverse diffusion step using the model predictions. At every step, the values of the observed channels are forcibly replaced with the true observed signals,

$$\boldsymbol{x_t^{(c)} = x_{obs}^{(c)}, \qquad \forall c \in C_{obs},}$$

thereby ensuring that the conditional constraints are always satisfied. As a result, the model performs stochastic restoration exclusively on the missing channels while preserving the observed channels without distortion.

Unlike pointwise prediction or simple interpolation, this conditional diffusion-based channel restoration model enables probabilistic reconstruction that jointly accounts for temporal structure and inter-channel correlations. Moreover, the same framework can be maintained even when the number or locations of observed channels change, simply by updating the conditional input and mask. This flexibility makes the proposed approach particularly well suited for BCI system design under electrode minimization constraints.

2.3. Channel Restoration Performance Evaluation

The restoration accuracy of the conditional diffusion–based EEG channel restoration model was analyzed at both the full-channel level and at separated levels for observed and unobserved channels. Performance was primarily interpreted in terms of signal reconstruction fidelity in the time domain and the preservation of inter-channel correlation structures.

Quantitative evaluation was conducted using mean squared error (MSE) and the Pearson correlation coefficient. MSE measures absolute amplitude reconstruc -tion error, while the correlation coefficient evaluates temporal waveform similarity and phase alignment independently of amplitude scale. All metrics were averaged over trials and time samples and then computed on a per-channel basis.

Across all 22 channels, the restoration achieved an overall MSE of 0.0578 and an overall correlation of 0.9656. These results indicate that the temporal structure of full EEG time series can be reconstructed with high fidelity using only low-channel observations. For the MI-9 channels used as conditional inputs, the restoration yielded an MSE of 0.0 and a correlation of 1.0, as the observed channel values were explicitly enforced at every reverse diffusion step. This confirms that the conditional diffusion process preserves observed signals without distortion.

For the remaining 13 unobserved channels targeted for restoration, the model achieved an average MSE of 0.0978 and an average correlation of 0.9418. Channel-wise analysis revealed lower reconstruction error and higher correlation in channels spatially adjacent to the central motor regions (C and CP series), whereas channels in portions of the parietal–occipital regions exhibited relatively higher error. This spatial variation suggests that the restoration reflects spatial and functional relationships with observed channels rather than relying on simple temporal interpolation.

Qualitative comparisons in the time domain further demonstrate that the restored signals closely follow the dominant oscillatory patterns and phase structures of the original EEG signals **(Figure 3)**. In a representative single-trial waveform comparison for the FC4 channel, the restored signal accurately reproduces overall amplitude scaling and temporal dynamics, with only limited discrepancies observed in localized high-frequency components. These differences can be interpreted as uncertainty inherent to the probabilistic restoration process and do not substantially affect the preservation of global rhythms and patterns.

Overall, the proposed conditional diffusion–based EEG channel restoration model achieves high correlation–based reconstruction for unobserved channels while fully preserving observed channels. These results demonstrate the model's effectiveness in mitigating spatial information loss in low-channel EEG settings and indicate its suitability as a reliable input signal foundation for subsequent motor imagery classification and robot control stages.

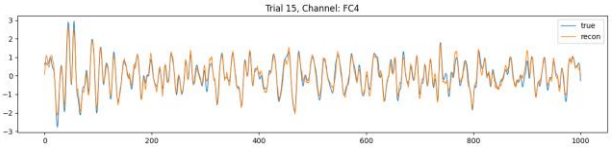

Fig. 3 Time-Domain comparison of original reconstructed EEG signals.

3. Motor Imagery EEG Classification Model

In this study, a state-of-the-art motor imagery (MI) EEG classification model reported to achieve strong performan -ce on standard MI-EEG benchmarks, including the BCIC IV-2a dataset, was adopted from the literature. Specifically, the classification model is based on the TCFormer architecture proposed by Altaheri et al.[11] This model integrates multi-kernel convolution–based early feature extraction, a Transformer encoder employing grouped-query attention, and a temporal convolutional

network (TCN) classification head with dilated causal convolutions. TCFormer has demonstrated consistent performance improvements over conventional CNN and CNN–Transformer hybrid models across multiple public MI-EEG datasets, including BCIC IV-2a.

The focus of this work is not on architectural modification or performance optimization of the classification model itself, but rather on analyzing how differences in input EEG representations affect motor imagery classification performance and subsequent robot control behavior. To this end, the classification model is kept fixed, and both low-channel EEG inputs and channel-restored EEG inputs are evaluated using the same classifier for direct comparison. This experimental design enables the effects of the channel restoration stage to be isolated from classification model design factors and provides a systematic basis for assessing how input signal quality propagates through the end-to-end pipeline, including the ROS2-based BCI robot control system.

3.1. Temporal Convolutional Transformer

TCFormer is designed as a hybrid architecture that combines convolution-based local feature extraction with Transformer-based global temporal context modeling, taking into account the non-stationary nature and low signal-to-noise ratio of EEG signals. The overall architect -tural flow of the model is illustrated in **Figure 4.**

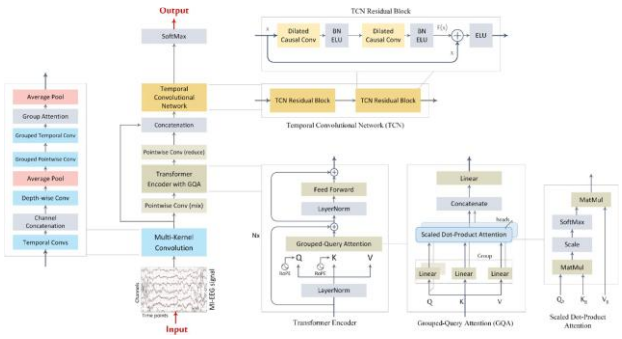

Fig. 4 Overall architecture of the TCFormer for motor imagery EEG classification. *Adapted from Altaheri et al.*

The input EEG time series $\boldsymbol{X} \in \boldsymbol{R}^{C \times T}$ is first processed by a multi-kernel convolutional block. In this block, temporal kernels of different lengths are applied in parallel to simultaneously capture neural activities at multiple temporal scales, such as the μ and β rhythms **(Figure 5)**. This multi-scale approach mitigates the limitations of single-kernel convolutions and enables effective separate -ion and emphasis of frequency band–specific information that is critical for motor imagery EEG analysis.

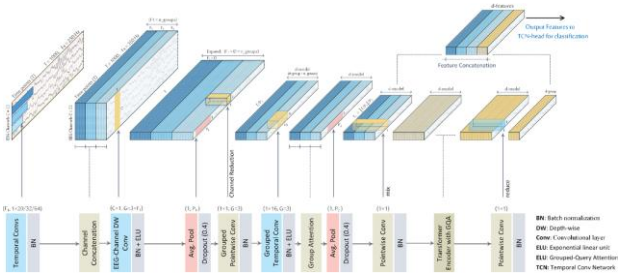

Fig. 5 Multi-kernel convolution block for multi-scale temporal feature extraction. *Adapted from Altaheri et al.*

The features extracted by the convolutional block are subsequently passed to a Transformer encoder to model global temporal dependencies. In TCFormer, grouped-query attention (GQA) is employed instead of standard multi-head self-attention. GQA is designed such that multiple query heads share key–value representations, thereby reducing computational complexity while effectively capturing long-range temporal relationships **(Figure 6)**. In addition, rotary positional embedding is applied to incorporate relative temporal relationships, enabling natural preservation of temporal order that is critical in EEG time-series modeling.

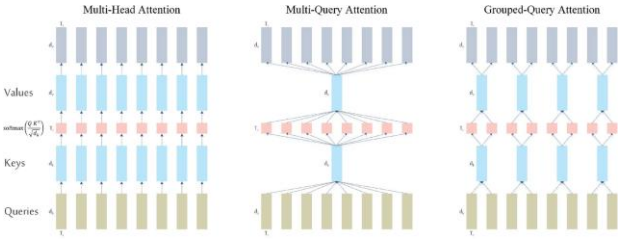

Fig. 6 Comparison of multi-head, multi-query, and grouped-query attention mechanisms. *Adapted from Altaheri et al.*

The output of the Transformer encoder is combined with convolution-based features and then fed into a TCN classification head. The TCN employs dilated causal convolutions to expand the receptive field along the temporal dimension, integrating both short- and long-term temporal patterns while preserving causality. Finally, logits for the motor imagery classes are generated based on the feature vector at the final time step.

In this manner, TCFormer sequentially integrates multi-scale convolution, an efficient global attention mechanism, and causal temporal decoding within a unified architecture. In this study, the TCFormer architecture is used as the

baseline classification model to analyze how changes in input EEG representations affect classification performan -ce and subsequent robot control stages.

3.2. Classification Performance Evaluation

Motor imagery (4-class) classification performance was analyzed primarily using accuracy and confusion matrices **(Figure 7)**. Accuracy was computed as the overall proportion of correctly classified samples in the test set. The confusion matrix was presented in a row-normalized (%) format with respect to the true class labels, enabling interpretation of class-wise misclassification patterns. During training, the training loss continuously decreased with increasing epochs, while the test loss exhibited a rapid initial drop followed by a gradual decrease, eventually converging in a stable manner. Correspondingly, classification accuracy improved progressively, reaching a final test accuracy of 71.10% with a test loss of 0.7561.

Class-wise accuracies (each class support = 130) were observed as follows: Class 0: 62.31%, Class 1: 75.97%, Class 2: 76.15%, and Class 3: 70.00%. Relatively higher classification performance was observed for Class 1 and Class 2. Analysis of the confusion matrix revealed that Class 0 was more frequently misclassified as Class 1 and Class 2, while Class 3 also exhibited a non-negligible level of confusion with Class 2 and Class 1. This behavior can be attributed to overlapping time–frequency characteristics among certain motor imagery classes, leading to closely formed decision boundaries.

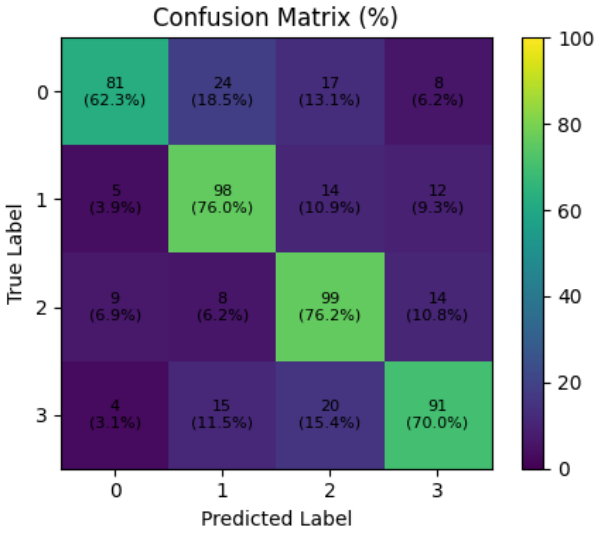

Fig. 7 Confusion matrix (%) of the 4-class motor imagery EEG classification on the test set. Values are normalized per true class.

The performance of the TCFormer-based classification model used in this study can be interpreted through comparison with existing motor imagery EEG classification literature that also employs the BCIC IV-2a dataset. For instance, Altaheri et al. reported classification accuracies ranging from approximately 62–63% to 83–85%, depending on the evaluation protocol, when applying the TCFormer architecture to the same dataset. In addition, numerous studies based on CNN, CNN–RNN, and CNN–Transformer architectures commonly report accuracies in the high-60% to low-70% range on BCIC IV-2a.[11] Within this context, the 71.10% classification accuracy achieved in this study represents a competitive performance level without degradation compared to existing classification models using the same dataset, and can be regarded as providing a stable baseline performance under standard MI-EEG classification settings.

In summary, the TCFormer-based classifier achieved approximately 71% accuracy for 4-class motor imagery classification under the experimental conditions of this study, placing it within a comparable or equivalent performance range relative to prior literature on BCIC IV-2a. Rather than targeting further optimization of the classifier itself, this model is used as a baseline to evaluate the impact of input differences before and after channel restoration, as well as to compare ROS2-based robot control performance in subsequent sections.

4. ROS2-Based BCI Robot Control System

4.1. End-to-End System Overview

The ROS2-based BCI robot control system proposed in this study is designed as an end-to-end pipeline that directly links EEG-based user intent inference to robot motion control, while incorporating a perception-based, limited safety filter to ensure operational safety in real-world environments. The core design principles of the system are as follows: (i) user intent remains the central element of control, (ii) no autonomous navigation functionality is included, and (iii) minimal intervention is performed only in hazardous situations.

The overall pipeline consists of three main stages. First, in the EEG-based BCI layer, motor imagery classification results are interpreted sequentially over time to generate robot motion intent. The classified MI classes (LEFT, RIGHT, FEET, TONGUE) are mapped to linear and

angular velocities according to predefined rules, and the resulting control commands are published to the /cmd_vel_bci topic. Commands generated at this stage represent pure user intent and do not incorporate any environmental information.

Second, in the environment perception layer, distance information acquired from an onboard LiDAR sensor is used to compute the minimum distance $\boldsymbol{d_{min}}$ to frontal obstacles. This value serves as an indicator of proximity to the most critical obstacle in the robot's current direction of motion. No path planning or goal-following is performed at this stage.

Third, in the intent–environment fusion layer, the BCI-based control commands and LiDAR-based risk indicators are combined to generate the final motion commands. This functionality is implemented in the env_filter node, which applies a rule-based policy defined by predefined thresholds $\boldsymbol{D_{safe}}$, $\boldsymbol{D_{stop}}$, and a deceleration coefficient $\boldsymbol{k}$, as summarized below:

- $\boldsymbol{d_{min}} > \boldsymbol{D_{safe}}$: execute user intent command
- $\boldsymbol{D_{stop}} < \boldsymbol{d_{min}} \leq \boldsymbol{D_{safe}}$: decelerate forward motion only
- $\boldsymbol{d_{min}} \leq \boldsymbol{D_{stop}}$: stop forward motion while preserving rotational intent

This design ensures that the robot's default behavior is always governed by user intent, while limited intervention is applied only in regions with collision risk. Accordingly, the safety filter is not intended to replace or bypass autonomous navigation algorithms, but rather to function as a protective mechanism that maximally preserves user intent.

The proposed system was validated in a Gazebo-based simulation environment. To enable repeated experiments under identical BCI command sequences and environment -tal conditions, ROS2 parameter files (YAML) and a rosbag-based recording and playback framework were employed. This setup ensures reproducibility of end-to-end control behavior and consistency of experimental results.

4.2. ROS2 System Architecture

The proposed BCI robot control system is composed of multiple functionally separated packages within a ROS2 workspace, each following a modular structure with clearly defined responsibilities. This design aims to enhance system scalability and ease of debugging, while simultaneously ensuring the reproducibility of the experimental results reported in this study.

The ROS2 workspace (ros2_ws/src) consists of five main packages. The bci_interface package is responsible for converting EEG-based user intent into robot control commands. It temporally replays sequences of motor imagery (MI) classes and publishes the corresponding commands to the /cmd_vel_bci topic. Class-specific velocity values, command durations, and related parameters are defined in YAML configuration files, enabling repeated reproduction of identical experimental conditions.

The env_filter package implements the environment-aware safety filter, which constitutes a core component of the proposed system. This node simultaneously subscribes to the /cmd_vel_bci topic and the LiDAR /scan topic. It computes the minimum forward obstacle distance $\boldsymbol{d_{min}}$ and generates the final /cmd_vel command according to a predefined rule-based policy. All deceleration thresholds and coefficients are managed as ROS2 parameters, allowing control policy adjustments without modifying source code.

The robot_description package contains URDF/Xacro files that define the robot's kinematic structure and sensor frames. **(Figure 8)** In this study, a differential-drive mobile robot configuration is assumed, and the Gazebo diff-drive plugin is configured to directly consume the /cmd_vel topic. By omitting a separate low-level control node, the control flow is simplified and the roles of the BCI layer and the environment safety filter are clearly delineated.

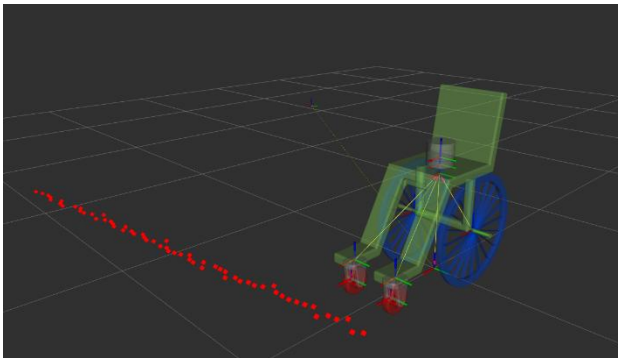

Fig. 8 RViz2 visualization of the BCI-controlled robot and LiDAR perception.

The robot_gazebo package manages the simulation environment, including Gazebo world files, LiDAR sensor configurations, and bridge settings for ROS–

Gazebo topic synchronization. **(Figure 9)** This setup ensures stable availability of the /scan and /clock topics within the ROS2 environment.

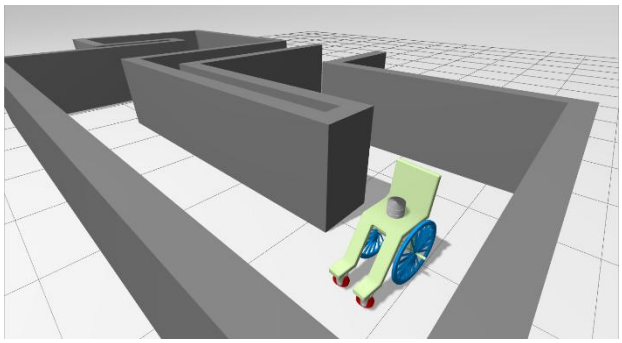

Fig. 9 Obstacle avoidance behavior in the Gazebo simulation environment.

Finally, the robot_bringup package serves as an integration layer for launching the entire system through a single launch file. This launch file simultaneously starts the Gazebo simulation, the BCI node, and the environment safety filter node, enabling the complete end-to-end control pipeline to be reproduced with a single command.

Fig. 10 ROS2 node–topic graph of the BCI robot control system.

Overall, this ROS2 architecture concentrates control logic within the BCI and safety filter layers, while delegating robot actuation and sensor handling to standard plugins. This approach achieves both structural simplicity and experimental reproducibility and provides a solid foundation for future extensions to real robotic platforms or online EEG inputs while preserving the same system interfaces.

5. Results

In this study, the end-to-end operation of the proposed ROS2-based BCI robot control system was validated in a simulation environment. The evaluation aims were threefold: (i) to verify that EEG-based user intent is stably transmitted to robot control commands, (ii) to confirm that the safety filter performs limited intervention while preserving user intent under hazardous environmental conditions, and (iii) to assess the reproducibility of experimental results under identical conditions.

First, robot behavior was analyzed in an environment without obstacles. Under this condition, the LiDAR-based minimum distance $\boldsymbol{d_{\min}}$ consistently remained above the safety threshold $\boldsymbol{D}_{\text{safe}}$, and the environment safety filter did not perform any intervention. Simulation results showed that the final control commands (/cmd_vel) numerically matched the BCI-based control commands (/cmd_vel_bci). Robot motions corresponding to motor imagery classes—such as forward motion, left and right rotation, and stopping—were reproduced in a temporally stable and predictable manner. These results demonstrate that the proposed system reflects user intent without distortion when no environmental constraints are present.

In environments with static obstacles, the computed $\boldsymbol{d_{\min}}$ from the LiDAR sensor decreased as the robot approached obstacles, triggering staged intervention by the environment safety filter. In the range $\boldsymbol{D}_{\text{stop}} < \boldsymbol{d_{\min}} \leq \boldsymbol{D}_{\text{safe}}$, the forward velocity component was reduced according to the deceleration coefficient $\boldsymbol{k}$. When $\boldsymbol{d_{\min}} \leq \boldsymbol{D}_{\text{stop}}$, forward motion was completely halted. Throughout this process, the angular velocity component was preserved, allowing user-intended rotational motion to be continuously executed. Consequently, the robot avoided collision risks while preserving user intent to the greatest extent possible. These results experimentally confirm that the safety filter is designed to perform only interpretable, rule-based interventions, rather than autonomous navigation or path planning.

To verify system reproducibility, repeated experiments were conducted under identical BCI command sequences and environmental configurations. In all experiments, velocity mappings and safety thresholds were fixed via ROS2 parameter files (YAML), and rosbag-based recording and playback were used to maintain identical input conditions. As a result, the timing of deceleration and stopping in the presence or absence of obstacles, as well as the robot's final positions, were consistently reproduced across repeated trials. The temporal evolution of control commands also remained identical. This demonstrates that the proposed ROS2-based architecture is well suited for explicit fixation of experimental conditions and repeated validation.

Robot behavior and sensor perception results were visually verified using RViz2 and the Gazebo simulation environment. In RViz2, the robot model, coordinate

frames, and LiDAR point clouds were used to confirm sensor integration and frame alignment. In the Gazebo environment, the robot's actual motion—decelerating and stopping while navigating an obstacle course—was directly observed. These end-to-end operation results are provided as supplementary video material, which records simulations conducted under the same experimental conditions described in this paper. The supplementary video is publicly available via a GitHub repository, with the repository address and access details provided in Section 7 (Data availability).

6. Conclusion

This study proposed an end-to-end BCI robot control system that mitigates information loss inherent in low-channel EEG environments through generative model–based channel restoration and connects the restored signals to motor imagery classification and ROS2-based robot control. Rather than focusing on performance gains of individual modules, the discussion emphasizes how system-level stability and reproducibility are achieved under the practical constraint of electrode minimization.

The conditional diffusion–based EEG channel restoration preserves observed channels while probabilistically compensating for the spatial information of unobserved channels, thereby maintaining the reliability of input signals for subsequent classification. This suggests that channel restoration should be interpreted not merely as a preprocessing technique, but as a representation recovery stage that alleviates structural information loss caused by electrode reduction.

In the motor imagery classification stage, a literature-based TCFormer model was adopted as a fixed baseline, enabling isolation of the effects of input EEG representation differences on overall system behavior. The achieved 4-class classification accuracy of approximately 71% falls within a competitive range compared to prior studies using the BCIC IV-2a dataset and provides a stable referen -ce point for subsequent robot control experiments.

Within the ROS2-based robot control system, user intent was placed at the center of control, and an intent-preserving safety filter was applied to perform limited intervention only under LiDAR-detected hazardous conditions. By preventing collisions while maintaining rotational intent, this structure mitigates the loss of user intent typically associated with safety interventions. In addition, the modular ROS2 archit -ecture and parameterized control policies jointly ensure experimental reproducibility and system scalability.

The limitations of this study include validation based on offline EEG data, the assumption of static obstacles, and evaluation confined to a simulation environment. Nevertheless, by combining generative model–based signal restoration under electrode minimization constraints with intent-preserving safety control, this work presents a practical system design direction for extending non-invasive BCI toward robotic control.

7. Data availability

All EEG datasets used in this study are publicly available. The BCIC IV-2a motor imagery EEG datasets can be downloaded from the BCI Competition IV repository: http://www.bbci.de/competition/iv/. Preproces -sing scripts, proposed conditional diffusion model (DDPM) and TCFormer models, and the ROS2 package configuration files used for end-to-end BCI robot control—including node implementations, launch files, parameter YAML files, and robot simulation descriptions are available at the following repository: https://github.co m/YoungwoongYoun/EEG-robotics.

References

(1) Flesher, S. N., Downey, J. E., Weiss, J. M., Hughes, C. L., Herrera, A. J., Tyler-Kabara, E. C., Boninger, M. L., Collinger, J. L., & Gaunt, R. A., 2021, "A Brain-Computer Interface that Evokes Tactile Sensations Improves Robotic Arm Control," *Science*, Vol. 372, No. 6544, pp. 831–836.

(2) Ding, Y., Udompanyawit, C., Zhang, Y., & He, B., 2025, "EEG-based brain-computer interface enables real-time robotic hand control at individual finger level," *Nature Communications*, Vol. 16, No. 1, Article 5401,

pp. 1–?, DOI: 10.1038/s41467-025-61064-x.

(3) Edelman, B. J., Meng, J., Suma, D., Zurn, C., Nagarajan, E., Baxter, B. S., Cline, C. C., & He, B., 2019, "Noninvasive neuroimaging enhances continuous neural tracking for robotic device control," *Science Robotics*, Vol. 4, No. 31, eaaw6844.

(4) Willett, F. R., Avansino, D. T., Hochberg, L. R., Henderson, J. M., & Shenoy, K. V., 2021, "High-performance brain-to-text communication via handwriting," *Nature*, Vol. 593, pp. 249–254.ssss

(5) Willsey, M. S., Shah, N. P., Avansino, D. T., Hahn, N. V., Jamiolkowski, R. M., Kamdar, F. B., Hochberg, L. R., Willett, F. R., & Henderson, J. M., 2025, "A high-performance brain–computer interface for finger decoding and quadcopter game control in an individual with paralysis," *Nature Medicine*, Vol. 31, pp. 96–104.

(6) Karpowicz, B. M., Ali, Y. H., Wimalasena, L. N., Sedler, A. R., Keshtkaran, M. R., Bodkin, K. L., Ma, X., Rubin, D. B., Williams, Z. M., Cash, S. S., Hochberg, L. R., Miller, L. E., & Pandarinath, C., 2025, "Stabilizing brain-computer interfaces through alignment of latent dynamics," *Nature Communications*, Vol. 16, No. 1, Article 4662, pp. 1–17.

(7) Sohl-Dickstein, J., Weiss, E. A., Maheswaranathan, N., & Ganguli, S., **2015**, "Deep Unsupervised Learning using Nonequilibrium Thermodynamics," *Proceedings of the 32nd International Conference on Machine Learning (ICML)*, PMLR Vol. 37, pp. 2256–2265; also arXiv:1503.03585 [cs.LG].

(8) Yang, L., Zhang, Z., Song, Y., Hong, S., Xu, R., Zhao, Y., Zhang, W., Cui, B., & Yang, M.-H., **2024**, "Diffusion Models: A Comprehensive Survey of Methods and Applications," *ACM Computing Surveys*, Vol. 56, No. 4, Article 105, pp. 1–39.

(9) Shah, M., & Patel, N., **2023**, "FNPG-NH: A Reinforcement Learning Framework for Flexible Needle Path Generation With Nonholonomic Constraints," *IEEE Robotics and Automation Letters*, Vol. 8, No. 99, pp. 5854–5861, DOI: 10.1109/LRA.2023.3300576.

(10) Luo, T.-j., & Cai, Z., **2025**, "Diffusion models-based motor imagery EEG sample augmentation via mixup strategy," *Expert Systems with Applications*, Vol. 262, Article 125585, pp. 1–18, DOI: 10.1016/j.eswa.2024.125585.

(11) Otarbay, Z., & Kyzyrkanov, A., **2025**, "SVM-enhanced attention mechanisms for motor imagery EEG classification in brain-computer interfaces," *Frontiers in Neuroscience*, Vol. 19, Article 1622847, pp. 1–18, DOI: 10.3389/fnins.2025.1622847.